JOC The Journal of Organic Chemistry

pubs.acs.org/joc Article

# Launching Graphene into 3D Space: Symmetry, Topology, and Strategies for Bottom-Up Synthesis of Schwarzites

Alexey V. Ignatchenko*

Cite This: J. Org. Chem. 2025, 90, 971−983 Read Online

ACCESS | Metrics & More | Article Recommendations | Supporting Information

**ABSTRACT:** Schwarzites are hypothetical carbon allotropes in the form of a continuous negatively curved surface with three-dimensional periodicity. These materials of the future attract interest because of their anticipated large surface area per volume, high porosity, tunable electric conductivity, and excellent mechanical strength combined with light weight. A three-decade-long history attempting schwarzite synthesis from gas-phase carbon atoms went without success. Design of schwarzites is both a digital art and the science of placing tiles of $sp^2$-carbon polygons on mathematically defined triply periodic minimal surfaces. The knowledge of how to connect polygons in sequence using the rules of symmetry unlocks paths for the bottom-up synthesis of schwarzites by organic chemistry methods. Schwarzite tiling by heptagons is systematically analyzed and classified by symmetry and topology. For the first time, complete plans for the bottom-up synthesis of many schwarzites are demonstrated. A trimer of heptagons is suggested as the key building block for most synthetic schemes.

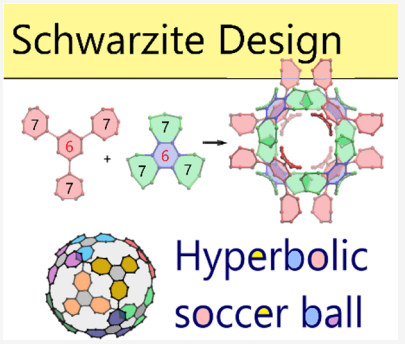




## 1. INTRODUCTION

The phenomenal rise of carbon allotropes such as graphene,[1] nanotubes,[2,3] and fullerenes[4] has been continuously offering technological advances in various fields, including photovoltaics,[5,6] batteries and supercapacitors,[7−10] membranes,[11,12] gas separation and storage,[13] chemical catalysis,[14−16] and electronic sensors.[17−19] It is quite fortunate that carbon nanotubes and fullerenes can be easily produced on an industrial scale by "brute force" methods—precipitation of carbon from the gas phase using metal catalysts or via an electric discharge between carbon electrodes—and that graphene can be economically produced by exfoliation from natural graphite sources.[1−4]

Schwarzites, a particularly elusive form of carbon allotropes, have generated considerable excitement although their synthesis remains unrealized. Introduced by McKay and Terrones over three decades ago,[20] schwarzites, named after German mathematician Karl Hermann Amandus Schwarz, are unique in their triple periodicity, possessing a beautiful symmetry that continues to fascinate physicists and material scientists around the world. Like their counterparts, these hypothetical carbon materials are supposed to consist of only $sp^2$-hybridized carbon atoms, with the striking difference that it would be a single piece of a continuous periodic surface filling the whole 3D space. Access to schwarzites would be analogous to achieving a tight packing of a single layer of graphene in 3D space by bending, twisting, and fitting it in without cutting it into pieces while enhancing its remarkable properties. According to numerous density functional theory (DFT) calculations, schwarzites might have superior mechanical strength,[21−26] light weight,[21,27−29] high porosity,[30] gas permeability,[31] and a tunable energy gap[32−34] between the valence and conduction bands, which is lacking in graphene.

The synthesis of schwarzites remains a challenging task that is fundamentally related to their negative Gaussian curvature. The spontaneous growth and termination of a positively curved surface of carbon atoms by closing to itself produces spherical fullerenes or cylindrical nanotubes as a converging process in which pieces with different curvatures can be separated afterward by fractionation. Growth at a constant zero curvature to a flat graphene is nonconverging and, therefore, infinite. In contrast, growth of a negatively curved triply periodic minimal surface (TPMS) from a gas-phase carbon is infinite but diverging.[35] Even if it could be seeded with a negatively curved element, its subsequent growth is possible in not just one but many ways, the exact number of which we do not know yet. Unlike fullerene spheres, TPMS growth does not terminate after surface edges meet, creating a closure. Instead, they continue facing a vast number of options. It is not only a different curvature that may form but also the type of TPMS or several types that might start growing simultaneously on different sides of a joined piece without a possibility for separation later. Not surprisingly, all attempts to grow spontaneously and attempts to isolate any schwarzite in the symmetrically pure state by brute

Received: June 14, 2024
Revised: October 25, 2024
Accepted: November 14, 2024
Published: November 21, 2024

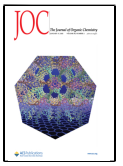

force methods have failed. The difficulty extends to the zeolite templating method, in which even the smallest mismatch between crystal lattice parameters of the zeolite template and the schwarzite or the presence of any residual hydrogen atoms inevitably leads to defects.[36,37]

Recent advances in the bottom-up synthesis of large-size polycyclic aromatic hydrocarbons (PAHs) have created a foundation of synthetic methods that may apply to the construction of novel carbon-based compounds and materials with exciting new topologies beyond plane nanographenes.[38−40] However, bottom-up synthetic strategies for a complete schwarzite molecular architecture have not been discussed in the literature. Currently, the only strategy for creating PAH with a negative curvature is narrowed down to the occasional inclusion of heptagons or octagons between benzene rings.[40−45] The opposite approach suggested in this work is to use heptagons or octagons as building blocks and join them to construct benzene rings in between. This study is intended to bring the attention of synthetic organic chemists to the needs of the research field traditionally dominated by solid-state physicists and material scientists. The goal is to analyze the symmetry and topology of various schwarzites that will allow us to choose the best strategy and to guide their bottom-up synthesis by organic chemistry methods.

## 2. RESULTS AND DISCUSSION

**2.1. Topology.** Planning for a bottom-up synthesis of schwarzites must start with a choice of a certain type of TPMS, the size of polygons, and a distinct tiling scheme. The most attractive synthetic targets are surfaces with a low genus and wider pores such as the well-known P, D, and G and a minor league H, HT, CLP, GW, or IWP. Examples of an ideal surface are shown in Figure 1, and tiling on various surfaces is illustrated throughout the paper. For the classification, description, and 3D models of TPMS, refer to Web sites of Brakke[46] and Schoen.[47]

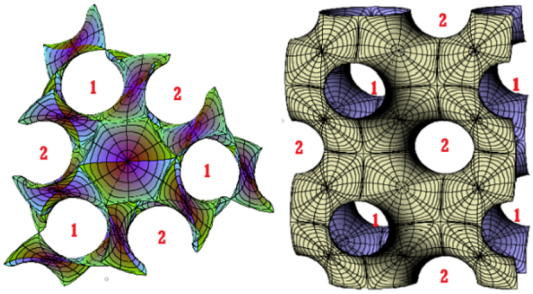


**Figure 1.** Balanced surfaces (G- and P- shown as examples) are recognized by two identical sides, 1 and 2, causing an equal-size diameter of channels connecting neighboring chambers.

Polygon tiles contributing to a negative curvature must have their size $N$ larger than six atoms, i.e., $N = 7$, 8, 9, or higher are suitable.[48] It is dictated by Euler's equation (eq 1)

$$V - E + F = 2(1 - g) \tag{1}$$

wherein $F$, $E$, and $V$ are the number of faces (i.e., polygons), edges, and vertices, respectively.[48,49] Genus, $g$, is related to the number of handles, i.e., pairs of openings in the unit cell. In the special case when all atoms are $sp^2$ hybridized carbon, each atom has three sigma bonds. Three cycles share one atom, and two cycles share one edge (bond), so that $2E = 3$ V. In this case, Euler's rule prescribes a certain number of polygons in the unit cell of a closed periodic structure having genus $g$ according to eq 2.[49]

$$\sum_N (6 - N) f_N = 12(1 - g) \tag{2}$$

For example, formula 2 predicts that $f_7 = 24$ heptagons ($N = 7$) or $f_8 = 12$ octagons ($N = 8$) will be required to construct a unit cell of the P-surface, which has genus $g = 3$. It may also be a combination of any size polygons, such as 4 octagons and 16 heptagons, or 26 heptagons and 2 pentagons. Pentagons create a positive curvature. Their presence levels off the negative curvature brought about by polygons with $N > 6$. Exactly 12 pentagons make spherical fullerenes according to eq 2 because a sphere has genus zero. Hexagons are excluded from the calculation since the 6-N term in such a case becomes zero; therefore, any number of hexagons may be used without affecting the curvature. Consequently, dilution by any number of hexagons is allowed for the bottom-up synthesis of negatively curved schwarzites, whereas mixing heptagons or octagons with four- or five-membered rings observed in some studies[45,50−54] is counterproductive.

Nondiluted structures composed of only octagons or heptagons have been described in the literature,[26,55,56] but their geometry looks highly strained for a carbon structure, and less accessible synthetically, similar to how C60 and C20 fullerenes are different.[57] The simplest way of isolating heptagons by dilution with a minimum number of hexagons is called the "hyperbolic soccer ball" pattern (Figure 2), which is

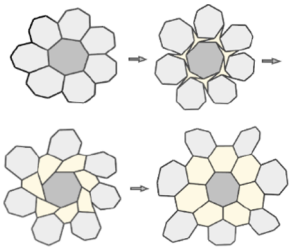

**Figure 2.** Leapfrog transformation from condensed heptagons to a hyperbolic soccer ball pattern.

like how pentagon rings in C60 fullerene are separated by hexagons.[34] A leapfrog transformation described by King[48] shows the relationship between a heptagon-only pattern and the hyperbolic soccer ball. In organic synthesis, a hypothetical [2 + 2 + 2] cycloaddition of three molecules of cycloheptene would create a hexagon ring. It is to the great advantage of such a bottom-up synthesis approach that no special care is needed for creating hexagons—they are created automatically by connecting six adjacent vertices of three heptagons. Thus, the hyperbolic soccer ball pattern, represented by the Schläfli symbol t{3,7}, or the vertex symbol [6.6.7],[58] may become the preferred way to construct schwarzites. It has long been recognized that a hyperbolic surface with genus 3 and 24 heptagons, i.e., 168 atoms, is equally important and analogous to the spherical surface fullerene that has 60 atoms.[48] Any further dilution by hexagons creates fullerenes with a higher number of atoms, such as C70, as well as schwarzites with >168 atoms in the unit cell for genus 3.

**2.2. Symmetry.** Mathematically ideal TPMS from the P, G, and D families are said to be balanced when two sides of the surface are equal (Figure 1). Two labyrinths on both sides of the balance surface created by the division of the whole space are


https://doi.org/10.1021/acs.joc.4c01503
J. Org. Chem. 2025, 90, 971−983

congruent. Tiling may not always be perfectly symmetrical, causing the distortion of the balance surface of tiles, hence leading to symmetry reduction. Such a distortion can be visually recognized by altering otherwise equal areas of openings 1 and 2 (Figure 1) that would become larger and smaller. A balanced tiling tends to have higher symmetry. Examples include **P7par**,[28] **P8**,[20] **G8Bal**, and **D8Bal**.[27] Tiling can be chiral, as in **D168**,[29] **P207-C168**, or **P130-C672**,[34] regardless of being balanced or not (Table S1). The nomenclature for schwarzites used in this work, in bold, consists of the TPMS type, symmetry group, chemical element symbol, and number of atoms in the unit cell. For enantiomeric surfaces, a (P) or (M) symbol may be added at the end depending on the positive (plus) or negative (minus) torsion angle of the propeller made of three heptagons located in corners of the cubic symmetry unit cell.

For TPMS with a cubic symmetry, such as the P-, G-, or D-surface, balanced tiling is easier to accomplish with eight-membered polygons amenable to the C4 rotation symmetry of a cube. Tiling with seven-membered polygons more often makes an unbalanced surface. Not surprisingly, the first discovered schwarzite, the Mackay–Terrones P-surface, was composed of octagons and it was balanced.[20] Related D- and G- surfaces based on octagon tiling were reported shortly thereafter.[27] Tiling of the D-surface by heptagons in the hyperbolic soccer ball pattern was described by Vanderbilt and Tersoff[29] in 1992, but it took another 30 years to find a solution with the same pattern for a P-surface.[34] G-Surface tiling by heptagons for the first time is shown below. Up-to-date information on new schwarzites can be found in the SACADA database[59] and on the Web site of the author's research group.[60]

To avoid the obvious mismatch between symmetries of a single heptagon and a cubic unit cell and to facilitate synthesis by using preassembled larger-size building blocks, heptagons can be combined in dimers and trimers (Figure 3). Trimers must be

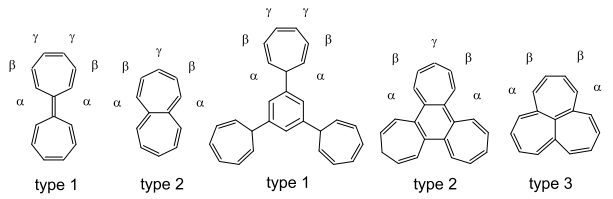


**Figure 3.** Types of heptagon dimers and trimers as building blocks for the bottom-up synthesis of schwarzites, classified by their connection to each other through one, two, or three vertices leaving alpha, beta, and gamma positions for interconnections.

placed on each of the eight corners of the cube and can be oriented according to the four C3 rotation axes, as, for example, on **P207-C168** (Figure 4). At the same time, unit cell tiling by heptagons can be viewed as placing a pair of dimers on each of the six faces of the cube and orienting them to obey C4 rotation symmetry. Either way, 8 × 3 or 6 × 4 tiling brings the same result, 24 heptagons, according to the total number required by Euler's equation (formula 2) for the unit cell.

The narrowest place of the P-surface is where two chambers join the edges of their openings, creating a neck (Figure 1). Let us introduce a topological characteristic of edges composing the neck useful for the net with point symbol {6.6.7}. If we define it as the number of carbon atoms on each heptagon of the chamber's opening exposed for connection with another chamber (Figure 4a), all six openings of the **P207-C168** small chamber will have the same configuration, (2222). Continuity of

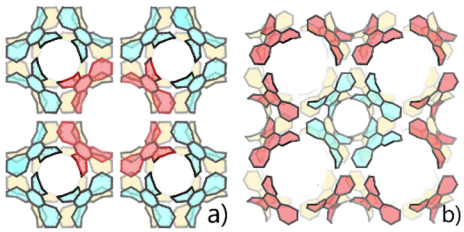


**Figure 4.** (a) Half of the **P207-C168** (unbalanced) surface large chamber is seen in the center between four small chambers (in the axial plane or eight in 3D). In its turn, (b) the small chamber is surrounded by eight large chambers. The surface serves as the border between chambers so that all small chambers are on one side, while large chambers are on the other side of the unbalanced surface.

the net with the same point symbol, i.e., by making hexagons between heptagons, dictates the configuration of the joined neighboring chamber also to be (2222), which classifies this configuration as self-complementary. While **P207-C168** is chiral, the neck configuration does not exhibit chirality, as explained below.

Other examples of self-complementary configurations for joining two cyclic chains of four heptagons are achiral (3131), chiral (3122), or chiral (4112), while (3311) taken as an example is not self-complementary because it requires (4121) to be paired with it when making hexagons in between two chains. These statements can be easily verified on paper by drawing the above configurations. The neck configuration is cyclically permuted; i.e., it may be written starting from any position forward in a circular way, while writing in a reverse order represents a mirror image. For example, writing (3122) is the same as (2312), while (3221) is their enantiomer. If the reverse writing makes a sequence different from the original, then it indicates chirality. For consistency, counting should be done in the same way, e.g., clockwise when viewing the chamber from outside, in a reverse lexicographic order, listing larger numbers first.

Self-complementary neck configurations are of particular importance for the design of schwarzites as the condition for periodicity by translational symmetry. Self-complementary configurations for the five heptagons include achiral (22222), chiral (31222), chiral (32122), chiral (31312), and achiral (33121). The achiral (33121) configuration is seen in the chiral **P130-C672**[34] model because neck chirality is a sufficient but not necessary requirement for the whole chamber or unit cell chirality. A partial list of self-complementary configurations with six heptagons is shown in the Supporting Information.

The most symmetric P-surface fitting within a cube corresponds to the following space groups: $P23$, $Pm\bar{3}$, $P432$, $P\bar{4}3m$, and $Pm\bar{3}m$, associated with group numbers 195, 200, 207, 215, and 221, respectively.[61] The most symmetric D-surface also exhibits a cubic symmetry and is associated with the following space groups and group numbers (in brackets): $F23$ (196), $Fm\bar{3}$ (202), $Fd\bar{3}$ (203), $F4_132$ (210), $F\bar{4}3m$ (216), $F\bar{4}3c$ (219), $Fm\bar{3}c$ (226), $Fd\bar{3}m$ (227), and $Fd\bar{3}c$ (228).[61] P and D surfaces may also exhibit tetragonal symmetry variants when the torus parameter, which characterizes the geometric and topological features of TPMS, deviates from its optimal cubic symmetry value of $\tau$ = 0.78. In contrast, the gyroid surface (G) is unique as it is considered to have only one symmetry form, $Ia\bar{3}d$ (group number 230). However, various tilings may exhibit lower symmetry. Unlike P and D surfaces, the gyroid is chiral, inherently leading to the chirality of all tilings. As described by


https://doi.org/10.1021/acs.joc.4c01503
J. Org. Chem. 2025, 90, 971−983

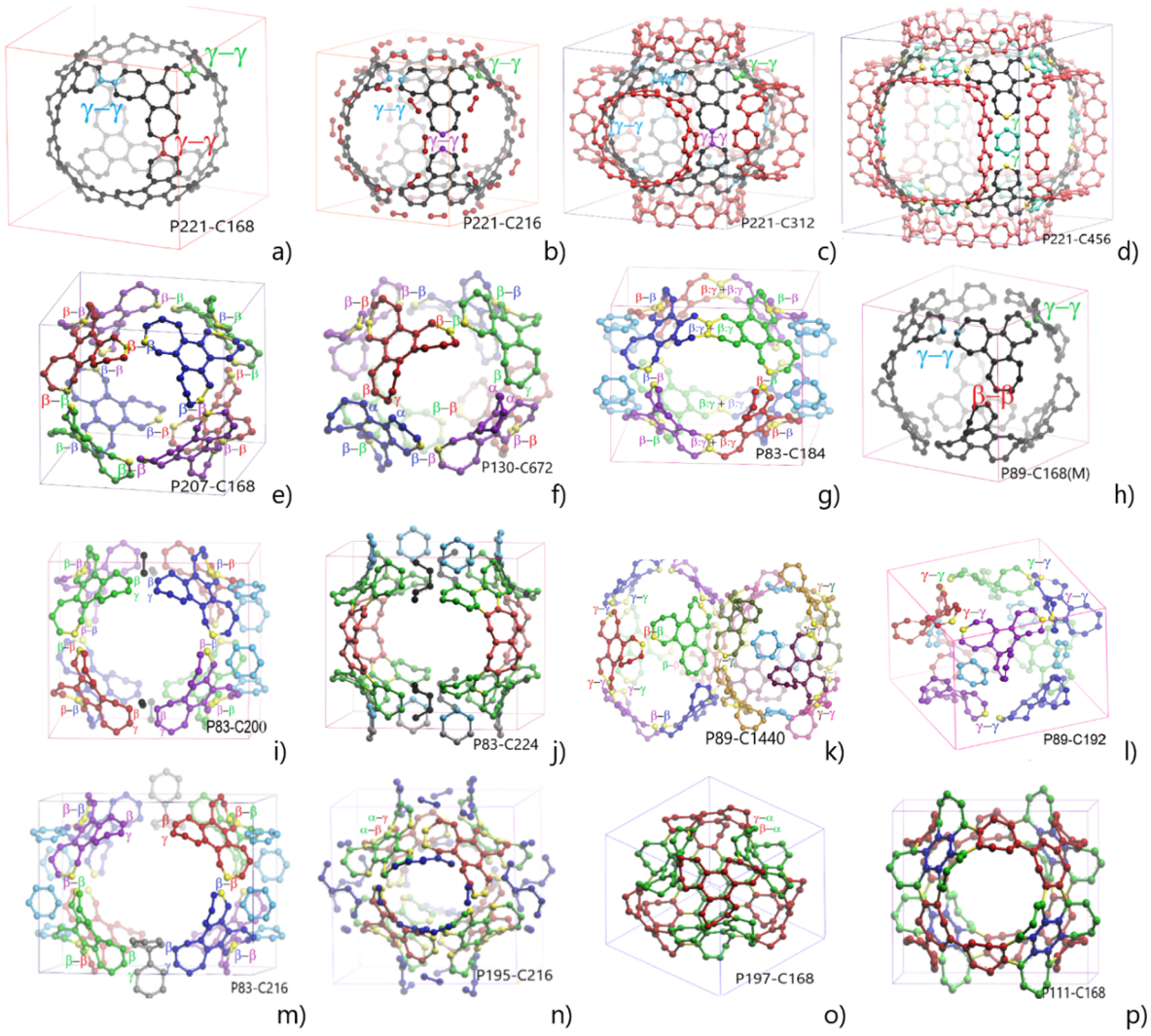


**Figure 5.** P-schwarzite tiling variety made by rotating type 2 heptagon trimers in eight corners of the unit cell while changing trimers' connections to each other through alpha, beta, or gamma carbon atoms. Different colors are used to represent possible building blocks for the bottom-up synthesis.

O'Keeffe, Hyde, and Proserpio, the gyroid's uniqueness lies in its 1111 transitivity properties, where it possesses a single distinct vertex, edge, face, and cell within its net, marking it as a structure of highest symmetry.[62]

A variety of P-surface tilings can be obtained by rotating heptagon trimers in eight corners of the unit cell cube and connecting them through either alpha, beta, or gamma positions (Table S1, Figures 5 and 6). The most symmetrical is the gamma-to-gamma connection within the unit cell for all three heptagons of the type 2 trimer (defined in Figure 3) leading to $Pm\bar{3}m$ symmetry, group 221. The remaining two carbon atoms, alpha and beta, from each of the four trimers on the cube's face, make the (22222222) chamber neck configuration to be used for connecting with the neighboring chambers, while the beta-to-beta connection would create a less symmetrical (31313131) configuration. The former case requires skewing to match the positions of the K region of one chamber opening and the bay regions of another chamber. Without skewing, direct contacts between both chamber's opposite K-regions create **P221-C168** with C4 and C8 rings between unit cells (Figure 5a), synthetically a very challenging structure, which departs from the hyperbolic soccer ball pattern. The skewed structure creates a pair of enantiomers of **P207−C168-*γ*** while reducing the symmetry to *P*432, group 207, and introducing chirality. Found to be highly strained and unstable by DFT calculations, this structure undergoes skeletal rearrangements. Therefore, tiling by gamma-to-gamma connections should materialize by adding more hexagons, e.g., joining the bay regions via a shared C2 fragment (**P221-C216**), or extra C6 rings (**P221-C312**, **P221-C456**) (Figure 5b−d), or any number of additional C6 rings, creating many more new tilings.

When type 2 heptagon trimers rotate in each corner of the cube, the symmetry is reduced, and naturally more stable tilings are produced via beta-to-beta connections either as the only type, creating a (31313131) neck configuration of **P207-C168** (Figure 5e), **P200-C276** (Figure S1i,j), or mixing *β*−*β* and *γ*−*γ* connections as in **P130-C672**, **P89-C168**, **P89-C192**, **P89-C1440**, sharing the *β*−*γ* edge, **P83-C184**, **P83-C224**, separating the *β*−*γ* edges by dilution, **P83-C200**, **P83-C216** (Figure 5f−m), or using alpha positions for chiral **P195-C216** and **P197-C168** (Figure 5n,o). A curious case is when two different kinds of chiral chambers in a group of eight in the unit cell create four diastereomers of **P89-C1440** (Table S1). Another interesting case is the mesochirality of **P111-C168**, which has a symmetry plane through pairs of chiral heptagons in each trimer, rendering this schwarzite achiral. Noteworthy, it utilizes another trimer


https://doi.org/10.1021/acs.joc.4c01503
J. Org. Chem. 2025, 90, 971−983

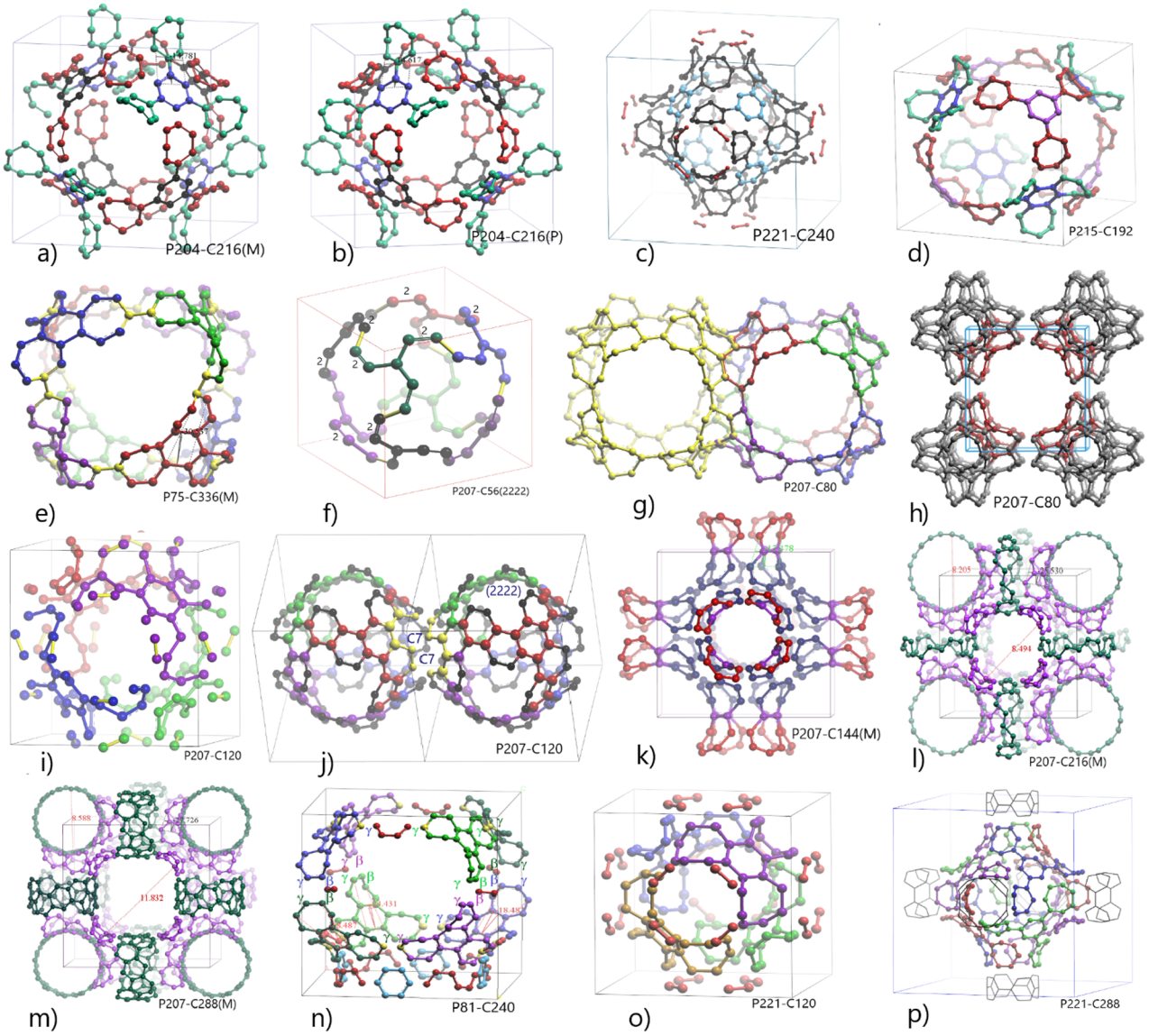


**Figure 6.** Various P-schwarzite tilings made by (a−d,p) type 1, (e,n) type 2, and (g) type 3 heptagon trimers, or (k−m) by heptagon dimers, or through sharing the edges of (f−j) heptagons or (o) octagons. Achiral schwarzites, like **P204-C216**, may have chiral tilings, like an enantiomeric (M) and (P) pair, (a,b). Coloring represents separate building blocks for a possible bottom-up synthesis.

type, 1,3-disubstituted C7-ring, by mixing it with type 2, shown in red and blue-green colors (Figure 5p). Similarly, rotation of type 1 trimers of the balanced chiral tiling **P204-C216** results in unbalanced achiral **P221-C240** or **P221-C288** (Figure 6a−c,p) with a (2222) neck configuration for interchamber connections. Type 1 and type 2 trimers can be mixed as in **P215-C192** (Figure 6d). Heptagon dimers sharing edges are utilized in chiral schwarzites **P207-C120**, **P207-C144**, **P207-C216**, and **P207-C288** (Figure 6i−m). Some schwarzites with edge-shared heptagons, **P207-C80**, or octagons, **P207-C56**, **P221-C120** (Figure 6f−h,o), may not allow tiling by trimers or dimers. In summary, variation of tilings can be obtained by adding hexagons, varying the dimer and trimer type, and varying their orientation in the cubic unit cell.

Each P-surface tiling has associated D- and G-surface tilings related via Bonnet rotation. For example, Video 1 (Supporting Information) shows the Bonnet transformation of **P197-C168** (Figure 5o) to **G199-C336** (Figure 7a). A systematic study of the schwarzites' relationship through Bonnet rotation will be reported separately. Selected examples of D, G, GW, H, HT, IWP, and CLP schwarzites are shown in Figure 7.

Like the P-surface, switching between beta-to-beta and gamma-to-gamma connections of type 2 trimers and their dilution by hexagons can be applied to other surfaces. For example, dilution by hexagons in **D227-C864(222222)** or **CLP131-C216** (Figure 7f,h) helps avoid skewing and strain. The beta-to-beta connection creates **D203-C672** or **CLP93-C168** (Figure 7b−d,p) without dilution. Dilution is a built-in feature of the type 1 trimer in **D227-C864(222)** (Figure 7e), **P221-C240**, **P204-C216** (Figure 6a−c), and **IWP204-C576** (Figure 7o). It can be applied to any tiling, even beta-to-beta-connected trimers, **D227-C960** (Figure 7g).

Remarkably, symmetry allows the number of beta-to-beta-connected trimers in opposite openings of a chamber to be 2, 3, 4, or 6, with the symmetries switching from cubic to hexagonal, and the surface type changing between **CLP93-C168**, **GW177-C252(313131)**, **P207-C168**, and **GW177-C252(222)**, respectively, with the same neck configuration (31313131) for the rest


https://doi.org/10.1021/acs.joc.4c01503
J. Org. Chem. 2025, 90, 971−983

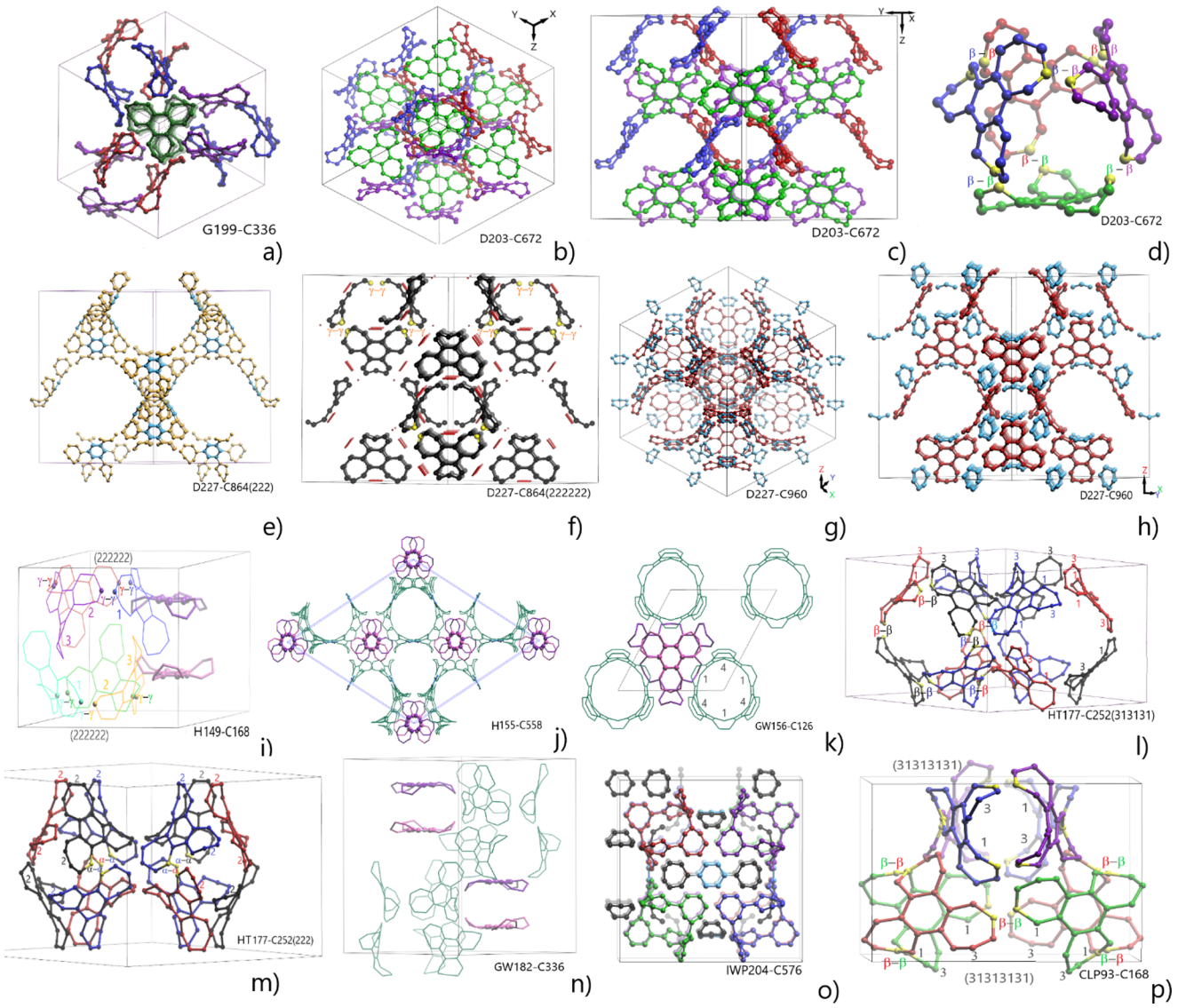


**Figure 7.** Examples of G, D, H, HT, GW, IWP, and CLP schwarzites using heptagon trimers type 2, (a) **G199-C336**, (b,c) **D203-C672**,[29] unit cell views, (d) single chamber, (e) type 1, **D227-C864(222)**, (f) type 2, **D227-C864(222222)**,[28] also called **D227-C216**,[34] (g) type 2, **D227-C960**, (h) **CLP131-C216**, (i−n) various hexagonal schwarzites with channels made of trimers (shown in green) linked by trimer pairs (shown in purple), (o) **IWP204-C576**, and (p) **CLP93-C168**. Various colors represent separate building blocks for a possible bottom-up synthesis.

of the openings (Figure 8). A similar array of tilings exists for the gamma-to-gamma connection of trimers, which requires their dilution.

## 3. SYNTHETIC STRATEGIES

**3.1. P-Surface.** Synthesizing PAH with rings larger than six atoms is a challenge, affecting schwarzites as well. Octagon-tiled schwarzites are highly symmetrical and balanced, while heptagon is not an easy-to-fit tile for the cubic symmetry possessed by most TPMS. Application of dimers and condensed trimers (type 3, Figure 3) not only satisfies the symmetry but also solves the problem of unpaired p-orbitals in the all-sp$^2$ heptagon hydrocarbon. For two other types of trimers, one or three carbon atoms with unpaired p-orbitals must be temporarily replaced by sp$^3$ atoms during the synthesis.

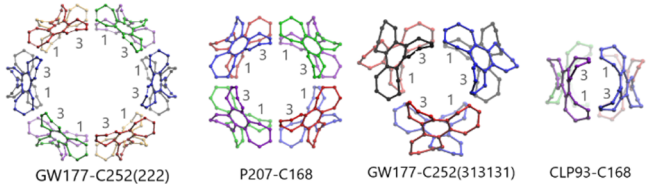


**Figure 8.** Number of beta-to-beta-connected trimers in a pair of chamber's opposite openings controls the surface type and symmetry.

While chambers of a balanced surface are uniformly sized, construction of unbalanced surfaces may start with either a large or a small chamber. The other size is created automatically, as exemplified by the **P207-C168** schwarzite[34] (Figure 4). Symmetry evokes several options for its assembly (Schemes 1 and 2). The size of the building block is doubled from one to eight trimers in three steps of Method 1 using the cross-coupling reaction between X and Y linking groups. Method 2 links trimers via para-to-para positions during the first cyclization, followed by a radical domino process[63] for sequential dimerization and the final cyclization during the unit cell assembly (Scheme 2).



https://doi.org/10.1021/acs.joc.4c01503
J. Org. Chem. 2025, 90, 971−983

**Scheme 1. P207-C168 Small Chamber Construction Strategy by Method 1**

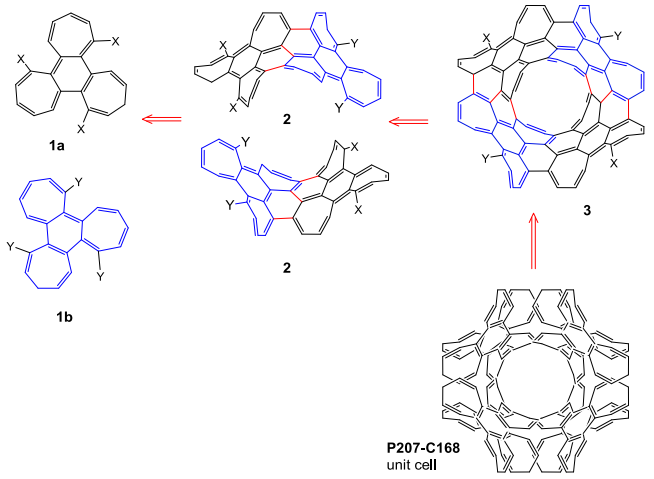


**Scheme 2. Alternative Strategy for P207-C168 Small Chamber Synthesis by Method 2, Cross-Coupling Heptagon Trimers and Subsequent Pairing through a Radical Domino Process**

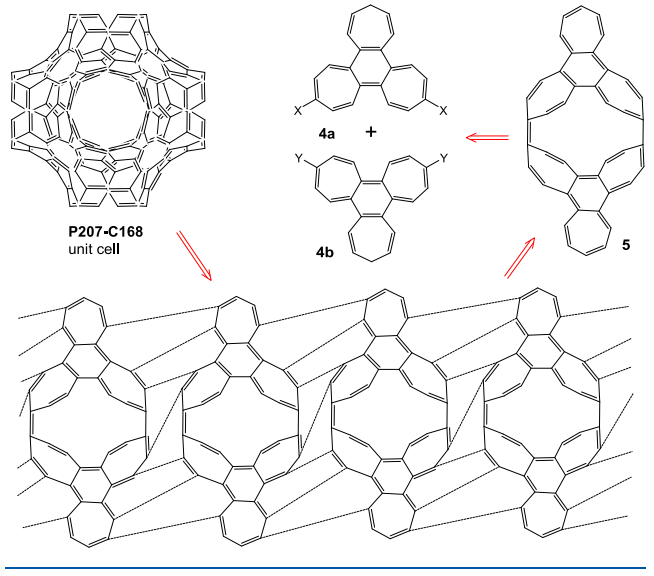


The final, most challenging task is to stack unit cell cubes in close-packed layers by connecting the chamber's openings, often three pairs at once, according to the terrace-step-kink (TSK) model.[64] Periodic organic material growth through precise covalent bonding with monomers in solution is unprecedented and significantly different from polymerization, crystal growth, or solvothermal synthesis of metal−organic frameworks. The latter proceed with a low concentration of defects because of reversible binding, unlike permanent covalent binding. Significant amounts of trial-and-error work lie ahead for testing different ideas. One example is elimination of neighboring $Me_3Si$- and $CF_3SO_3$- groups to generate triple bonds by Kobayashi's method[65−67] and connect alkynyl carbons in a cascade zipping reaction (Scheme 3). While there is no such precedent in the literature, this reaction has a reasonable expectation to proceed based on the constraint of each alkyne bond position in space essential for cascade cyclization reactions.[68] Because of the stepwise cascade mechanism,

**Scheme 3. Potential Extension of Kobayashi's Method of Alkyne Generation In Situ for Joining Small Chambers of P207-C168, Neck Configuration (2222)**

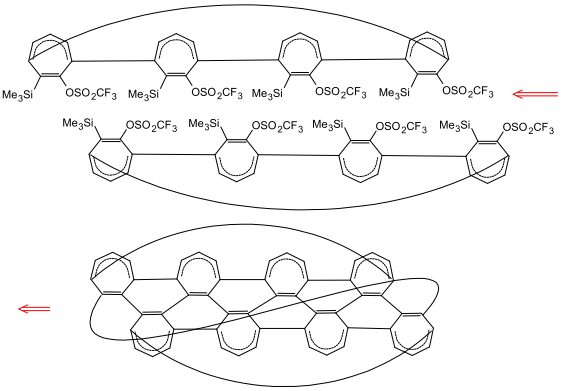

Hückel's 4N + 2 rule for concerted electrocyclic reactions does not apply in this case.

The **P207-C168** large chamber with the achiral neck configuration (313131)^6 can be made by method 1 (Scheme 4) via the beta-to-beta connection of trimers. The whole surface

**Scheme 4. Proposed Synthesis of the P207-C168 Large Chamber by Method 1**

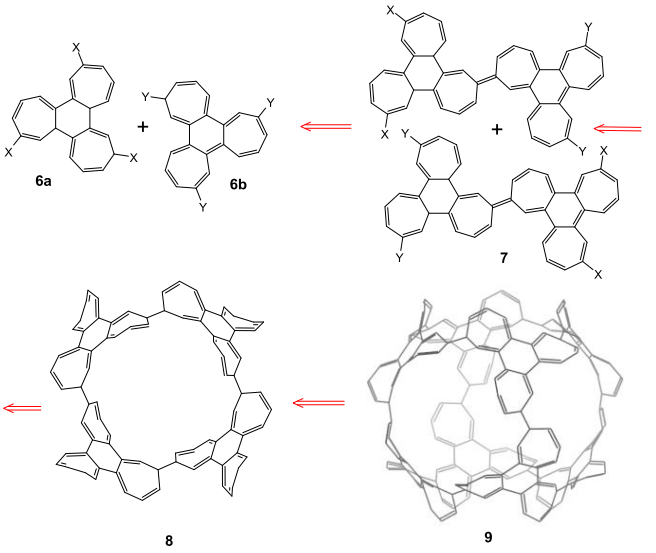


is chiral, and chiral heptagon trimers must be used for its construction in a pure enantiomeric form. Fast racemization of propeller-like trimers with chirality defined by the torsion angle in Figure 9 is expected in solution due to a shallow inversion barrier reminiscent of [7]-circulene.[69] Racemization becomes impossible when the enantiomer configuration is fixed through step 2 cyclization. The chirality challenge adds to the complexity of schwarzite synthesis. Mixing up enantiomers violates the symmetry and makes growth in the desired direction impossible. The best strategy is to separate enantiomers after step 1 when larger fragments experience a higher inversion barrier or after step 2 when racemization becomes impossible (Figure 10).

A point system can quantify the complexity of a synthetic design. Assigning one point for each cyclization step and one for managing chirality, the complexity index for both methods 1−2 in producing **P207-C168** is three. To minimize the number of cyclization steps, a simpler method could initially join four


https://doi.org/10.1021/acs.joc.4c01503
J. Org. Chem. 2025, 90, 971−983

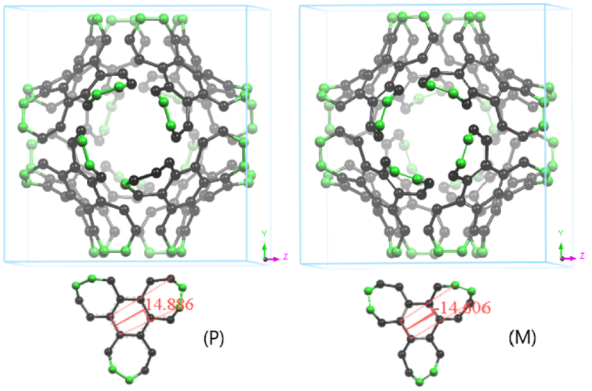


**Figure 9.** (P) and (M) enantiomers of hexagon trimers from **P207-C168** characterized by positive (plus) and negative (minus) torsion, defined as shown for the propeller-like shape, +14.8° and −14.8°, respectively.

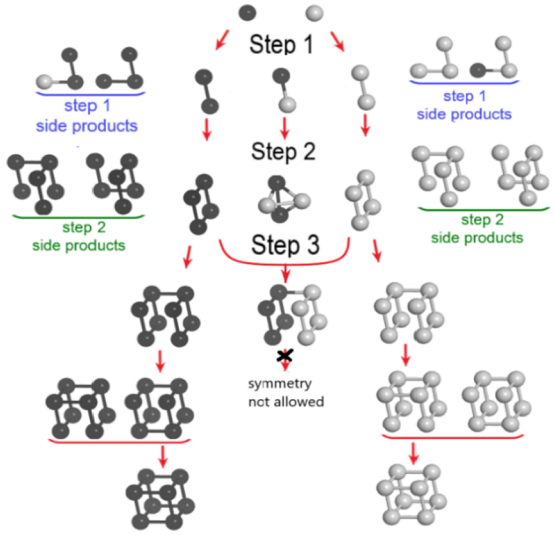


**Figure 10.** Stepwise construction of a chiral surface by method 1 requires the separation of enantiomers. Dark and light balls represent the two enantiomers of the heptagon trimer building block.

trimers, making two sets (**10a** and **10b** in Scheme 5) positioned at opposite corners of the unit cell cube body diagonal.

Both intermediates **10ab** assume spherical shapes resembling half-chambers during geometry optimization via molecular mechanics. By coupling two sets, the entire chamber can be formed in a single cyclization, bringing the complexity index down to two. Another advantage of method 3 is the ability to control the selectivity of each group of four trimers' formation by varying the ratio 1a:1b. A 3:1 excess of either trimer selectively creates the **10a** or **10b** intermediate, while methods 1−2 may suffer from competing linear oligomerization alongside cyclization.

Application of method 3 for achiral schwarzite synthesis, such as **P215-C192** (Scheme 6), brings the complexity index down to 1. Six bonds must be created during the single cyclization step (Scheme 7). Molecular modeling shows that two intermediates, **15** and **16**, adopt the hemisphere shape required for cyclization after aromatization of the not-so-much curved **13** and **14**. Both reactions can be done in one pot since there is a literature precedent for a $Pd(OAc)_2$-catalyzed oxidative Heck process coupled with dehydrogenation by DDQ.[70] Each of the two types of trimers in **P215-C192**, structures **11** and **12**, are surrounded

**Scheme 5. Method 3 for the Construction of the P207-C168 (Chiral) Small Chamber**

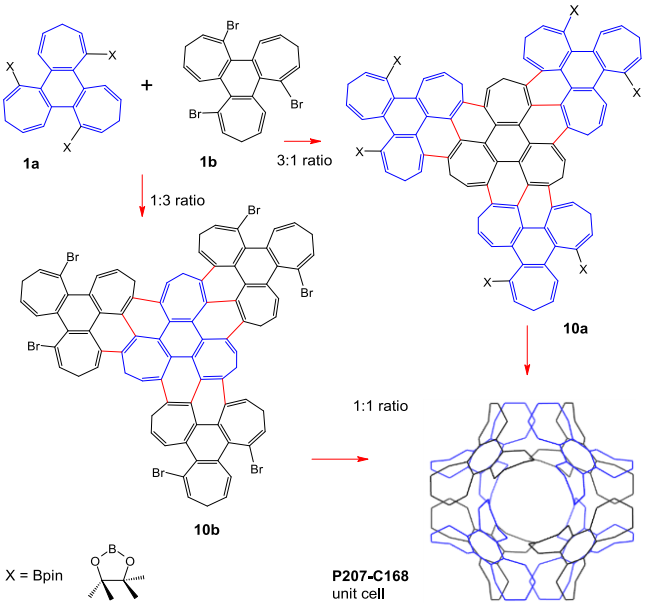


**Scheme 6. Proposed Construction of Two Halves of the P215-C192 Unit Cell from Two Kinds of Trimers Applying a Principle of Excess of One over the Other**[a]

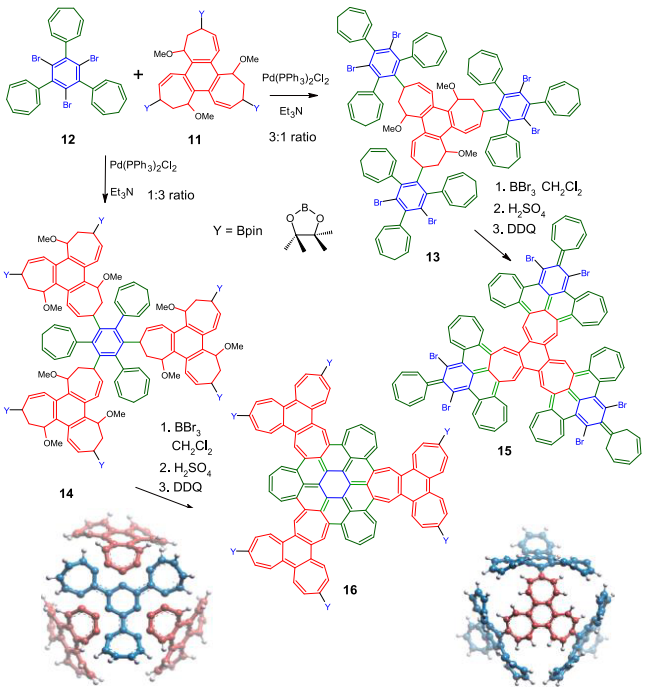


[a]Three trimers of each type surround the other one in the **P215-C192** unit cell as illustrated.

by three trimers of the other kind as emphasized by the illustration in Scheme 6. Worth mentioning, there are achiral schwarzites, **P204-C216**, **P221-C240**, and **P221-C288**, but their tiling is chiral with two options of different enantiomeric trimers of type 1.

Method 3 is applicable to the synthesis of other schwarzites, even those as challenging as **P207-C56(2222)**, composed of octagons sharing edges (Figure 6f and Scheme 8). The unit cell


https://doi.org/10.1021/acs.joc.4c01503
J. Org. Chem. 2025, 90, 971−983

**Scheme 7. Cyclization Step for the P215-C192 Unit Cell Assembly**

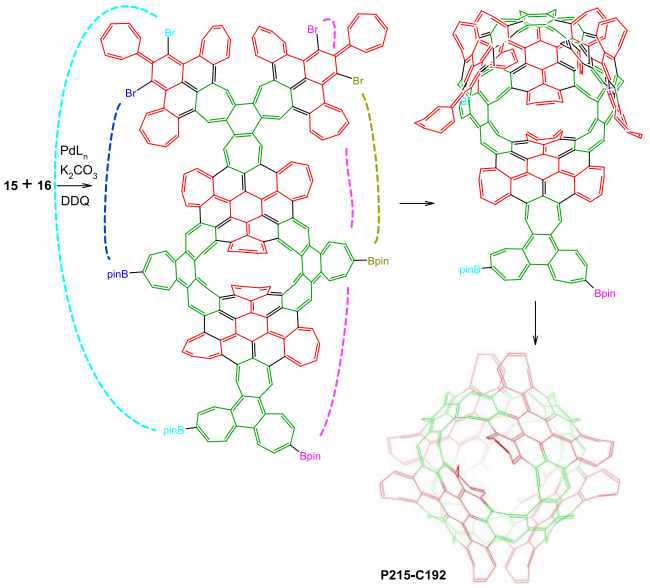


**Scheme 8. Proposed Synthetic Design of the P207-C56(2222) Large Chamber by Method 3**[a]

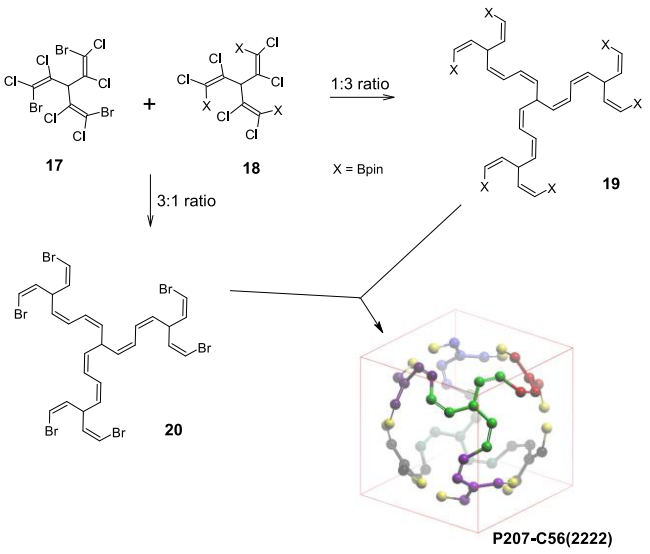


[a]Chlorine atoms (omitted for clear viewing) are essential for joining unit cells into a periodic structure.

synthesis in this case gets complexity index 1, but it must create octagons when joining unit cells, possibly by the Ullmann reaction, as well as dehydrogenate $sp^3$ atoms in each corner of the unit cell. Interestingly, changing the trans position of the Br atom to the cis makes **P207-C56(1^8)** schwarzite (Scheme S2), which is unstable according to DFT computation.

In a variation of method 3 applied for the **P207-C120** synthesis design, cyclization may take place between two unequally sized pieces, **23b** and **24**, prepared through benzyne trimerization (Scheme 9). It might be possible to make a **P207-C120** unit cell in a one-pot reaction starting from trimer **24**, or even monomer **21**. Schemes 8 and 9 both imply C7-ring formation only during the step of joining unit cells.

Octagons too can be combined in trimers and spaced out at the four diagonal corners of the cube, totaling 12 heptagons in

**Scheme 9. Proposed Synthesis of the P207-C120 Large Chamber through Benzyne Trimerization, Stepwise via 23b, or Directly from Four Molecules 24**

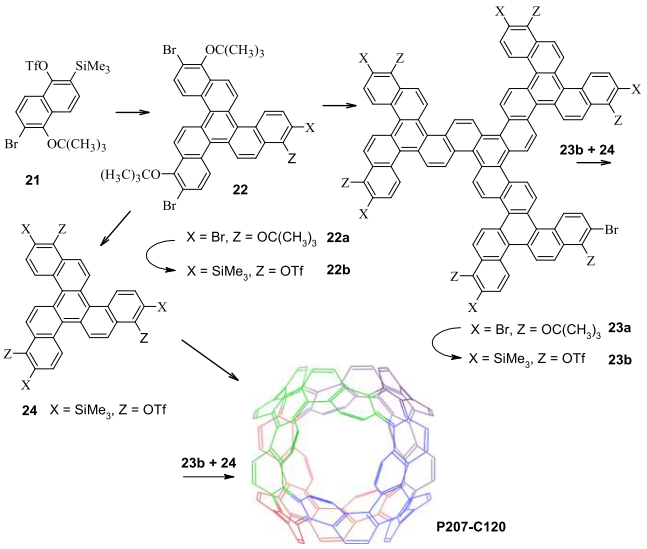


the unit cell according to Euler's formula. C2 fragments added between unit cells of **P221-C120** (shown in red, Figure 6o) must stay on just three faces of the cube, making unsymmetrical chambers difficult but still possible to synthesize (Scheme 10). A

**Scheme 10. P221-C120 Design**

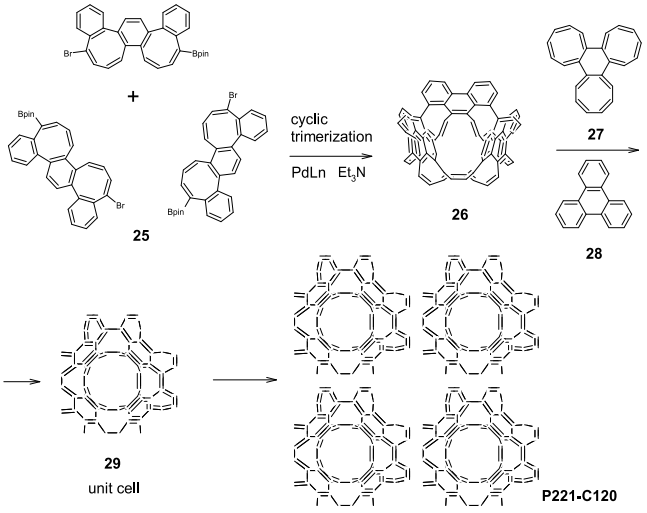


plan of complexity 3 suggests joining three dimers **25** into the first cycle of six octagons and then adding two nonequal-sized trimers as top and bottom covers. The last three octagons result from the addition of the small cover, **28**. Another way of dealing with unsymmetrical chambers is to make one larger than the unit cell (Scheme 11). Four dimers of **30** create a barrel, **33**. Three barrels join through benzyne trimerization into a half-chamber. Two half-chambers join into the small chamber **35**, serving as the periodic superelement and easing off TSK limitations. Tilings shown in Figures 5−7 suggest synthetic designs for most other schwarzites.

**3.2. D-Surface.** Making the whole chamber, large or small, in just one cyclization is proposed for **D227-C960** construction (Scheme 12) using Suzuki coupling and Diels−Alder benzyne condensation for gamma-to-gamma or alpha-to-alpha trimers **36**


https://doi.org/10.1021/acs.joc.4c01503
J. Org. Chem. 2025, 90, 971−983

**Scheme 11. P221-C216 Design**

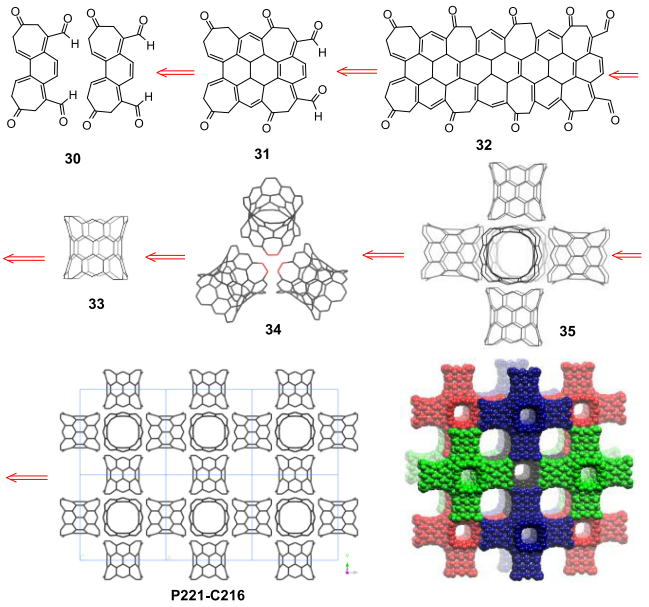


**Scheme 12. D227-C960 Chamber Design**

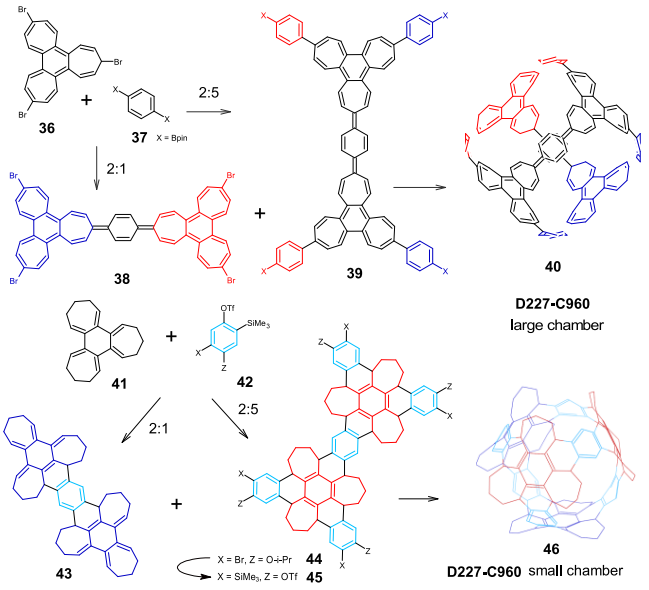


**Scheme 13. D227-C1248 Synthesis Design via Diels–Alder Condensation**

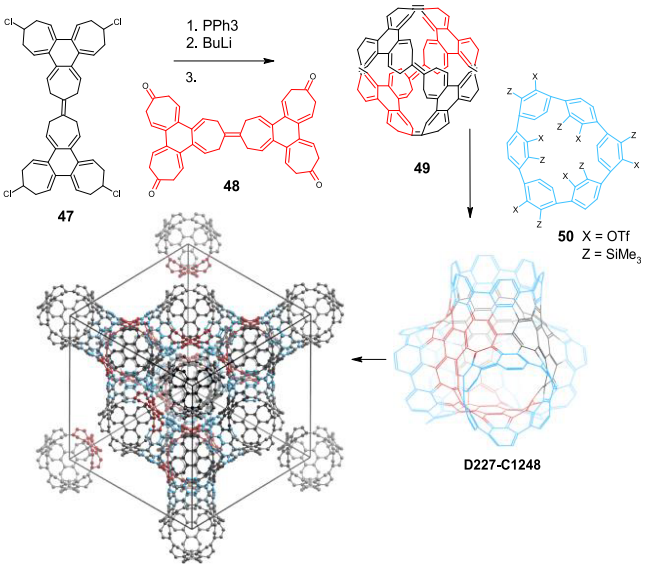


**Scheme 14. Design for D227-C864(222222) Synthesis via Suzuki Coupling**

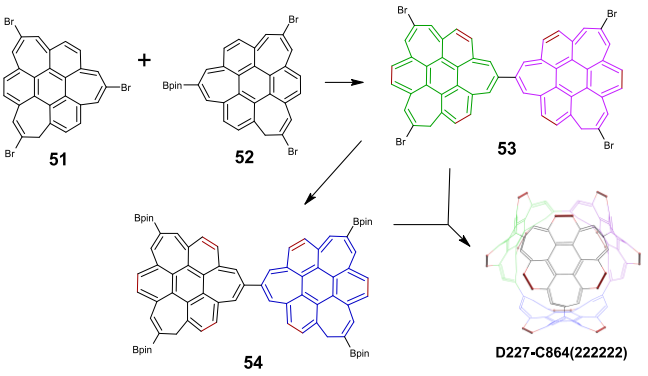


and **41**, connections, respectively, with the synthesis complexity at level 1. Dehydrogenation of the Diels–Alder product with DDQ is required for aromatization.

P-, D-, and G-chambers constructed by gamma-to-gamma trimer connection can be joined by various lengths (n,n) of armchair nanotubes, offering an infinite number of molecular architectures. Two strategies shown in Schemes 13 and 14 use [6]-cycloparaphenylene **50** for **D227-C1248** or the C2 fragments built-in trimers **51**–**52** for **D227-C864(222222)** synthesis. Benzyne Diels–Alder reaction is proposed for attaching nanotubes to chambers. Additional examples of molecular architectures with nanotubes are shown in the Supporting Information.

**3.3. G-Surface.** Classification of the connection type between trimers in P-chambers extends to the G-surface. Thus, the $\alpha$:$\alpha$ + $\beta$:$\gamma$ type seen in **P197-C168** can be used for making related (via Bonnet rotation) G-schwarzite **G199-C336** by method 3 (Scheme 15), joining trimers **55** and **56** in a 3:1 ratio into half-chamber **57** and pairing with the other similarly constructed half-chamber, **61**.

**3.4. CLP Surface.** Synthetic design of the simplest representative, the **CLP93-C168** chamber (Scheme 16), proposes one cyclization between type 2 trimer beta carbons, taking advantage of a higher reactivity of bromine vs chlorine and $B(OH)_2$ vs $BF_3K$ in Suzuki–Miyaura coupling.[71] Less reactive groups will be utilized for joining chambers together, while the rest of the bonds can be accomplished by dehydrogenation. Dilution by hexagons (**CLP131-C216**, Scheme S5) requires a larger set of building blocks and higher complexity.

**3.5. IWP and Hexagonal Symmetry Surfaces.** Synthesis of the **IWP204-C576** chamber might be possible from a single monomer **68** using different reactivity groups in stages. Less reactive Cl and $BF_3K$ will be used for the final stage, connecting cube corners into the periodic structure (Scheme 17).

As a general strategy for schwarzites with hexagonal symmetry, each chamber connects to three others. The **GW156-C126** chamber can be prepared by joining two groups of six heptagons. Chambers **72** are linked by heptagon dimers **73** to form a periodic structure (Scheme 18). A great variety of


https://doi.org/10.1021/acs.joc.4c01503
J. Org. Chem. 2025, 90, 971–983

**Scheme 15. G199-C336 Chamber, Half Unit Cell Design**

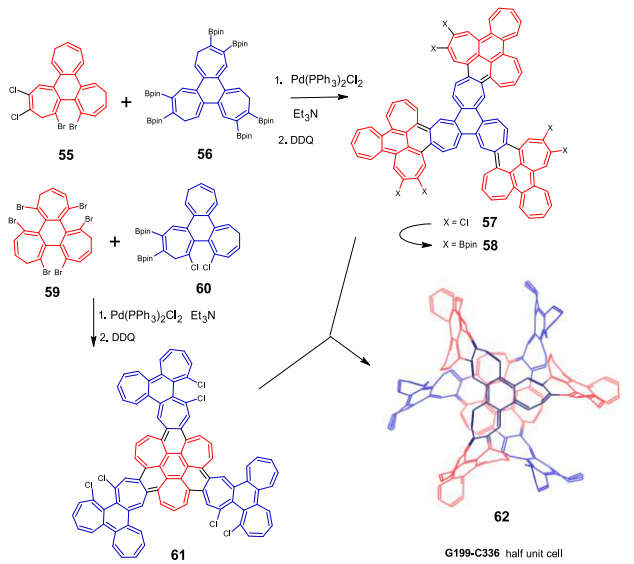


**Scheme 16. CLP93-C168 Chamber Design**

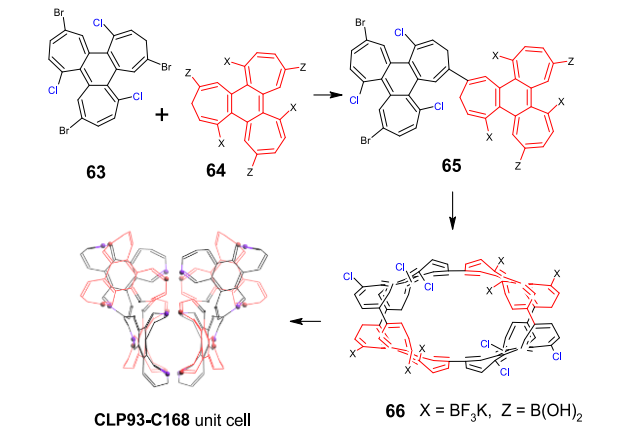


**Scheme 17. IWP204-C576 Design**

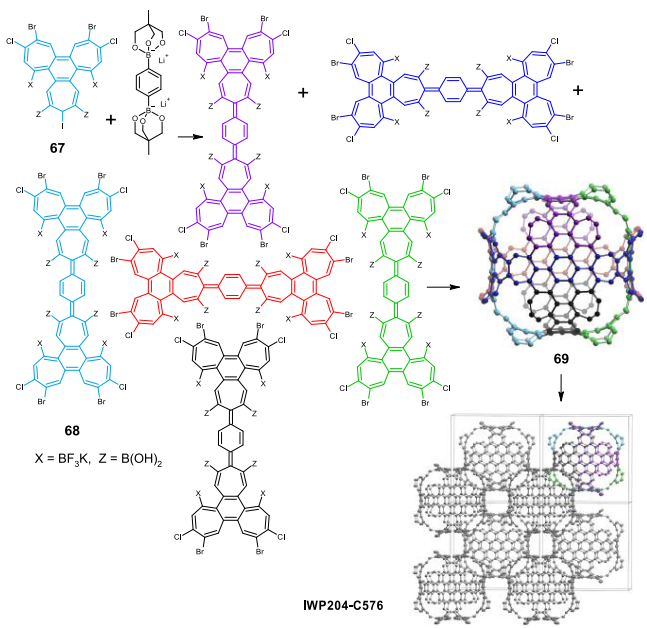


hexagonal symmetry H, HT, and GW schwarzites can be made by varying the chambers and linking units (Table S1).

**Scheme 18. GW156-C126 Design**

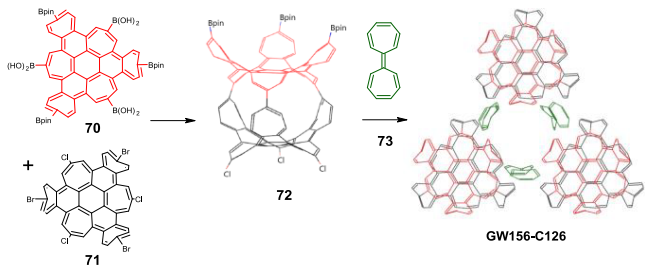


In summary, synthetic methods such as Diels–Alder and radical domino additions as well as Ullmann, Suzuki, and Heck couplings can be used for making schwarzites, apart from the Scholl reaction,[40,41] which may lead to the C7 to C6 ring rearrangement.

## 4. CONCLUSIONS

Systematically performed analysis of schwarzites demonstrates that the bottom-up synthesis utilizing strategically selected heptagon or octagon trimers holds a greater potential for controlling a wider array of topologies, geometries, and pore size distributions in periodic carbon materials compared to templating on zeolites. Specific synthetic approaches must be devised and tested, with the major challenge being the assembly of chambers into periodic structures. Understanding the topology and symmetry provides the guiding principles needed to succeed in synthesis. Proof of concept for the bottom-up synthesis of defect-free periodic materials has yet to be demonstrated, but the growing interest in schwarzites ensures that the stepwise approach using synthetic building blocks will gain traction. Most promising synthetic targets include unit cells for schwarzites **D227-C960**, **P215-C192**, **P207-C56(2222)**, **P207-C120**, **G199-C336**, and **CLP93-C168**, achievable by level 1 synthetic complexity.

## 5. EXPERIMENTAL SECTION

**5.1. Computational Method.** Periodic structures were constructed, and DFT calculations were carried out by using the CASTEP software package from Dassault Systèmes Biovia Corp. Graphical representations were generated using Materials Studio.

Geometry and unit cell optimization for each periodic structure were performed using CASTEP within the generalized gradient approximation for electron exchange and correlation, employing the PBE functional as described by Perdew et al.[72] The Tkatchenko–Scheffler exchange correlation was additionally incorporated to address dispersive interactions.[73,74] All calculations were conducted with spin restriction, and relativistic effects were included using the Koelling–Harmon scalar treatment for pseudopotential generation.

A plane-wave energy cutoff of 600 eV was applied, and the Brillouin zone was sampled using the Monkhorst–Pack scheme with a $2 \times 2 \times 2$ grid. Structural relaxation continued until the change in total energy was less than 0.00002 atomic units, with SCF density and gradient convergence criteria set to 0.00001 and 0.004 atomic units, respectively.

**Topology analysis** was performed, and standard nomenclature for point symbols, vertex symbols, and tiling (as listed in Table S1) was generated using ToposPro software, following the recommendations outlined in ref 58.



https://doi.org/10.1021/acs.joc.4c01503
J. Org. Chem. 2025, 90, 971−983

## ■ ASSOCIATED CONTENT

### Data Availability Statement

The data underlying this study are available in the published article and its Supporting Information.

### Supporting Information

The Supporting Information is available free of charge at https://pubs.acs.org/doi/10.1021/acs.joc.4c01503.

Partial list of self-complementary neck configurations; table with the list of schwarzites and data on their symmetry, geometry, and topology; additional figures of some schwarzites and synthetic schemes; identification of hexagonal schwarzites; and molecular architectures extended with nanotubes (PDF)

Bonnet rotation between structures **P197-C168** and **G199-C336** (AVI)

## ■ AUTHOR INFORMATION


### Corresponding Author

**Alexey V. Ignatchenko** − *Chemistry Department, St. John Fisher University, Rochester, New York 14618, United States;* orcid.org/0000-0002-7806-6857; Email: aignatchenko@sjf.edu, Alexey.Ignatchenko@gmail.com

Complete contact information is available at: https://pubs.acs.org/10.1021/acs.joc.4c01503


### Notes

The author declares no competing financial interest.

## ■ ACKNOWLEDGMENTS

The author dedicates his work to the memory of scientists who suffered from current wars. The author is grateful for the support and resources received from St. John Fisher University (SJF), the Lavery Library, and the Chemistry department. The author deeply thanks Dr. Ken Brakke (Susquehanna University Prof. Emeritus), Dr. Mark McKinzie (Math Dept., SJF), Sam Acosta (2023 SJF graduate with B.S. degree in Math), and Dr. Humberto Terrones (Rensselaer Polytechnic Institute) for useful discussions and help with modeling. Support from the NSF grant 1955130 for the shared use of Materials Studio software and a high-performance computer is greatly acknowledged.

## ■ ABBREVIATIONS

TPMS, triply periodic minimal surface; PAH, polycyclic aromatic hydrocarbons; DFT, density functional theory; TSK, terrace-step-kink

## ■ REFERENCES


(1) Urade, A. R.; Lahiri, I.; Suresh, K. S. Graphene Properties, Synthesis and Applications: A Review. *JOM* **2023**, *75* (3), 614−630.

(2) Anzar, N.; Hasan, R.; Tyagi, M.; Yadav, N.; Narang, J. Carbon Nanotube - A Review on Synthesis, Properties and Plethora of Applications in the Field of Biomedical Science. *Sensors International* **2020**, *1*, No. 100003.

(3) Rathinavel, S.; Priyadharshini, K.; Panda, D. A Review on Carbon Nanotube: An Overview of Synthesis, Properties, Functionalization, Characterization, and the Application. *Materials Science and Engineering: B* **2021**, *268*, No. 115095.

(4) Yadav, J. Fullerene: Properties, Synthesis and Application. *Res. Rev. J. Phys.* **2018**, *6* (3), 1−6.

(5) Ganesamoorthy, R.; Sathiyan, G.; Sakthivel, P. Review: Fullerene Based Acceptors for Efficient Bulk Heterojunction Organic Solar Cell Applications. *Sol. Energy Mater. Sol. Cells* **2017**, *161*, 102−148.

(6) Kumari, M. A.; Swetha, T.; Singh, S. P. Fullerene Derivatives: A Review on Perovskite Solar Cells. *Materials Express* **2018**, *8* (5), 389−406.

(7) Balogun, M.-S.; Luo, Y.; Qiu, W.; Liu, P.; Tong, Y. A Review of Carbon Materials and Their Composites with Alloy Metals for Sodium Ion Battery Anodes. *Carbon N Y* **2016**, *98*, 162−178.

(8) Cheng, Q.; Tang, J.; Ma, J.; Zhang, H.; Shinya, N.; Qin, L.-C. Graphene and Carbon Nanotube Composite Electrodes for Supercapacitors with Ultra-High Energy Density. *Phys. Chem. Chem. Phys.* **2011**, *13* (39), 17615−17624.

(9) Kumar, H.; Sharma, R.; Yadav, A.; Kumari, R. Recent Advancement Made in the Field of Reduced Graphene Oxide-Based Nanocomposites Used in the Energy Storage Devices: A Review. *J. Energy Storage* **2021**, *33*, No. 102032.

(10) Yu, W.; Yoshii, T.; Aziz, A.; Tang, R.; Pan, Z.-Z.; Inoue, K.; Kotani, M.; Tanaka, H.; Scholtzová, E.; Tunega, D.; Nishina, Y.; Nishioka, K.; Nakanishi, S.; Zhou, Y.; Terasaki, O.; Nishihara, H. Edge-Site-Free and Topological-Defect-Rich Carbon Cathode for High-Performance Lithium-Oxygen Batteries. *Advanced Science* **2023**, *10* (16), No. 2300268.

(11) Gkika, D. A.; Karmali, V.; Lambropoulou, D. A.; Mitropoulos, A. C.; Kyzas, G. Z. Membranes Coated with Graphene-Based Materials: A Review. *Membranes* **2023**, *13* (2), 127.

(12) Bhol, P.; Yadav, S.; Altaee, A.; Saxena, M.; Misra, P. K.; Samal, A. K. Graphene-Based Membranes for Water and Wastewater Treatment: A Review. *ACS Appl. Nano Mater.* **2021**, *4* (4), 3274−3293.

(13) Gadipelli, S.; Guo, Z. X. Graphene-Based Materials: Synthesis and Gas Sorption, Storage and Separation. *Prog. Mater. Sci.* **2015**, *69*, 1−60.

(14) Machado, B. F.; Serp, P. Graphene-Based Materials for Catalysis. *Catal. Sci. Technol.* **2012**, *2* (1), 54−75.

(15) Fan, X.; Zhang, G.; Zhang, F. Multiple Roles of Graphene in Heterogeneous Catalysis. *Chem. Soc. Rev.* **2015**, *44* (10), 3023−3035.

(16) Prakash, S. H.; Roopan, S. M. A Comprehensive Review on Recent Developments in the Graphene Quantum Dot Framework for Organic Transformations. *J. Organomet. Chem.* **2023**, *997*, No. 122790.

(17) Gergeroglu, H.; Yildirim, S.; Ebeoglugil, M. F. Nano-Carbons in Biosensor Applications: An Overview of Carbon Nanotubes (CNTs) and Fullerenes (C60). *SN Appl. Sci.* **2020**, *2* (4), 603.

(18) Nag, A.; Mitra, A.; Mukhopadhyay, S. C. Graphene and Its Sensor-Based Applications: A Review. *Sens Actuators A Phys.* **2018**, *270*, 177−194.

(19) Yusof, N. A.; Abd Rahman, S. F.; Muhammad, A. Chapter 9 - Carbon Nanotubes and Graphene for Sensor Technology. In *Synthesis, Technology and Applications of Carbon Nanomaterials*; Rashid, S. A.; Raja Othman, R. N. I.; Hussein, M. Z., Eds.; Elsevier: 2019; pp 205−222.

(20) Mackay, A. L.; Terrones, H. Diamond from Graphite. *Nature* **1991**, *352* (6338), 762.

(21) Miller, D. C.; Terrones, M.; Terrones, H. Mechanical Properties of Hypothetical Graphene Foams: Giant Schwarzites. *Carbon N Y* **2016**, *96*, 1191−1199.

(22) Bastos, L. V; Ambekar, R. S.; Tiwary, C. S.; Galvao, D. S.; Woellner, C. F. Mechanical Energy Absorption of Architecturally Interlocked Petal-Schwarzites. *Carbon Trends* **2023**, *13*, No. 100299.

(23) Woellner, C. F.; Botari, T.; Perim, E.; Galvão, D. S. Mechanical Properties of Schwarzites - A Fully Atomistic Reactive Molecular Dynamics Investigation. *MRS Adv.* **2018**, *3* (8−9), 451−456.

(24) Felix, L. C.; Gaál, V.; Woellner, C. F.; Rodrigues, V.; Galvao, D. S. Mechanical Properties of Diamond Schwarzites: From Molecular Dynamics Simulations to 3D Printing. *arXiv* 2020. .

(25) Felix, L. C.; Ambekar, R.; Tromer, R. M.; Woellner, C. F.; Rodrigues, V.; Ajayan, P. M.; Tiwary, C. S.; Galvao, D. S. Schwarzites and Triply Periodic Minimal Surfaces: From Pure Topology Mathematics to Macroscale Applications. *Small* **2024**, No. 2400351.

(26) Hyde, S. T.; O'Keeffe, M. At Sixes and Sevens, and Eights, and Nines: Schwarzites P3, p = 7, 8, 9. *Struct Chem.* **2017**, *28* (1), 113−121.
(27) Terrones, H.; Terrones, M. Curved Nanostructured Materials. *New J. Phys.* **2003**, *5*, 126.
(28) Lenosky, T.; Gonze, X.; Teter, M.; Elser, V. Energetics of Negatively Curved Graphitic Carbon. *Nature* **1992**, *355* (6358), 333−335.
(29) Vanderbilt, D.; Tersoff, J. Negative-Curvature Fullerene Analog of C60. *Phys. Rev. Lett.* **1992**, *68* (4), 511−513.
(30) Jiang, J.; Klauda, J. B.; Sandler, S. I. Hierarchical Modeling $O_2$ and $N_2$ Adsorption in $C_{168}$ schwarzite: From Quantum Mechanics to Molecular Simulation. *J. Phys. Chem. B* **2004**, *108* (28), 9852−9860.
(31) Borges, D. D.; Galvao, D. S. Schwarzites for Natural Gas Storage: A Grand-Canonical Monte Carlo Study. *MRS Adv.* **2018**, *3* (1), 115−120.
(32) Han, M. Y.; Özyilmaz, B.; Zhang, Y.; Kim, P. Energy Band-Gap Engineering of Graphene Nanoribbons. *Phys. Rev. Lett.* **2007**, *98* (20), No. 206805.
(33) Benedek, G.; Bernasconi, M.; Cinquanta, E.; D'Alessio, L.; De Corato, M. The Topological Background of schwarzite Physics. In *Mathematics and Topology of Fullerenes*; Springer: 2011.
(34) Ignatchenko, A. V.; Willower, J. P. Schwarz P-Surface via Isolated Sp2 Carbon Heptagons: Design and Properties. *J. Comput. Chem.* **2023**, *44* (9), 954−961.
(35) Lijima, S.; Ichihashi, T.; Ando, Y. Pentagons, Heptagons and Negative Curvature in Graphite Microtubule Growth. *Nature* **1992**, *356* (6372), 776−778.
(36) Chi, S.; Kim, C.; Lee, Y.; Choi, M. Diversity in Atomic Structures of Zeolite-Templated Carbons and the Consequences for Macroscopic Properties. *JACS Au* **2024**, *4*, 1489.
(37) Taylor, E. E.; Garman, K.; Stadie, N. P. Atomistic Structures of Zeolite-Templated Carbon. *Chem. Mater.* **2020**, *32* (7), 2742−2752.
(38) Wang, M.-W.; Fan, W.; Li, X.; Liu, Y.; Li, Z.; Jiang, W.; Wu, J.; Wang, Z. Molecular Carbons: How Far Can We Go? *ACS Nano* **2023**, *17* (21), 20734−20752.
(39) Zhang, Y.; Yang, D.; Pun, S. H.; Chen, H.; Miao, Q. Merging a Negatively Curved Nanographene and a Carbon Nanoring. *Precision Chemistry* **2023**, *1* (2), 107−111.
(40) Zhang, Y.; Pun, S. H.; Miao, Q. The Scholl Reaction as a Powerful Tool for Synthesis of Curved Polycyclic Aromatics. *Chem. Rev.* **2022**, *122* (18), 14554−14593.
(41) Pun, S. H.; Miao, Q. Toward Negatively Curved Carbons. *Acc. Chem. Res.* **2018**, *51* (7), 1630−1642.
(42) Pun, S. H.; Chan, C. K.; Luo, J.; Liu, Z.; Miao, Q. A Dipleiadiene-Embedded Aromatic Saddle Consisting of 86 Carbon Atoms. *Angew. Chem., Int. Ed.* **2018**, *57* (6), 1581−1586.
(43) Cheung, K. Y.; Chan, C. K.; Liu, Z.; Miao, Q. A Twisted Nanographene Consisting of 96 Carbon Atoms. *Angew. Chem., Int. Ed.* **2017**, *56* (31), 9003−9007.
(44) Cheung, K. M.; Xiong, Y.; Pun, S. H.; Zhuo, X.; Gong, Q.; Zeng, X.; Su, S.; Miao, Q. Negatively Curved Molecular Nanocarbons Containing Multiple Heptagons Are Enabled by the Scholl Reactions of Macrocyclic Precursors. *Chem.* **2023**, *9* (10), 2855−2868.
(45) Chaolumen; Stepek, I. A.; Yamada, K. E.; Ito, H.; Itami, K. Construction of Heptagon-Containing Molecular Nanocarbons. *Angew. Chem., Int. Ed.* **2021**, *60* (44), 23508−23532.
(46) Brakke, K. *Ken Brakke's Home Page*. https://kenbrakke.com/ (accessed Jan 18, 2024).
(47) Schoen, A. H. *Alan Schoen geometry*. https://schoengeometry.com/e-tpms.html (accessed Dec 18, 2023).
(48) King, R. B. Chemical Applications of Topology and Group Theory. 29. Low Density Polymeric Carbon Allotropes Based on Negative Curvature Structures. *J. Phys. Chem.* **1996**, *100* (37), 15096−15104.
(49) O'Keeffe, M.; Adams, G. B.; Sankey, O. F. Predicted New Low Energy Forms of Carbon. *Phys. Rev. Lett.* **1992**, *68* (15), 2325−2328.
(50) Zhu, C.; Shoyama, K.; Niyas, M. A.; Würthner, F. Supramolecular Substructure of C60-Embedded schwarzite. *J. Am. Chem. Soc.* **2022**, *144* (36), 16282−16286.
(51) Kawasumi, K.; Zhang, Q.; Segawa, Y.; Scott, L. T.; Itami, K. A Grossly Warped Nanographene and the Consequences of Multiple Odd-Membered-Ring Defects. *Nat. Chem.* **2013**, *5* (9), 739−744.
(52) King, B. T. Nanographenes Do the Twist. *Nat. Chem.* **2013**, *5* (9), 730−731.
(53) Kirschbaum, T.; Rominger, F.; Mastalerz, M. A Chiral Polycyclic Aromatic Hydrocarbon Monkey Saddle. *Angew. Chem., Int. Ed.* **2020**, *59* (1), 270−274.
(54) Gao, Q.; Ou, L.; Hu, Z. Architecture Design of Novel Carbon Family: Polyhedra as Building Blocks. *Carbon Trends* **2023**, *11*, No. 100256.
(55) Hyde, S. T.; Cramer Pedersen, M. schwarzite Nets: A Wealth of 3-Valent Examples Sharing Similar Topologies and Symmetries. *Proceedings of the Royal Society A: Mathematical, Physical and Engineering Sciences* **2021**, *477* (2246), 20200372.
(56) He, C.; Sun, L.; Zhang, C.; Zhong, J. Two Viable Three-Dimensional Carbon Semiconductors with an Entirely Sp2 Configuration. *Phys. Chem. Chem. Phys.* **2013**, *15* (2), 680−684.
(57) Wang, Z.; Ke, X.; Zhu, Z.; Zhu, F.; Ruan, M.; Chen, H.; Huang, R.; Zheng, L. A New Carbon Solid Made of the World's Smallest Caged Fullerene C20. *Phys. Lett. A* **2001**, *280* (5), 351−356.
(58) Blatov, V. A.; O'Keeffe, M.; Proserpio, D. M. Vertex-, Face-, Point-, Schläfli-, and Delaney-Symbols in Nets, Polyhedra and Tilings: Recommended Terminology. *CrystEngComm* **2010**, *12* (1), 44−48.
(59) Hoffmann, R.; Kabanov, A. A.; Golov, A. A.; Proserpio, D. M. Homo Citans and Carbon Allotropes: For an Ethics of Citation. *Angew. Chem., Int. Ed.* **2016**, *55* (37), 10962−10976.
(60) Ignatchenko, A. *Schwarzites, Dr. Alexey Ignatchenko Research Group webpage*. http://citadel.sjfc.edu/faculty/aignatchenko/schwarzites.html (accessed Oct 21, 2024).
(61) Ros, A. Isoperimetric Inequalities in Crystallography. *Journal of the American Mathematical Society* **2004**, *17*, 373−388.
(62) Hyde, S. T.; O'Keeffe, M.; Proserpio, D. M. A Short History of an Elusive Yet Ubiquitous Structure in Chemistry, Materials, and Mathematics. *Angew. Chem., Int. Ed.* **2008**, *47* (42), 7996−8000.
(63) Tietze, L. F.; Brasche, G.; Gericke, K. M. Radical Domino Reactions. In *Domino Reactions in Organic Synthesis*; John Wiley & Sons, Ltd: 2006; pp 219−279.
(64) Burton, W. K.; Cabrera, N.; Frank, F. C. The Growth of Crystals and the Equilibrium Structure of Their Surfaces. *Philos. Trans. R. Soc. London, A* **1951**, *243*, 299−358.
(65) Shi, J.; Li, L.; Li, Y. O-Silylaryl Triflates: A Journey of Kobayashi Aryne Precursors. *Chem. Rev.* **2021**, *121* (7), 3892−4044.
(66) Chen, L.; Zhang, C.; Wen, C.; Zhang, K.; Liu, W.; Chen, Q. Gold-Catalyzed Cyclotrimerization of Arynes for the Synthesis of Triphenylenes. *Catal. Commun.* **2015**, *65*, 81−84.
(67) Peña, D.; Escudero, S.; Pérez, D.; Guitián, E.; Castedo, L. Efficient Palladium-Catalyzed Cyclotrimerization of Arynes: Synthesis of Triphenylenes. *Angew. Chem., Int. Ed.* **1998**, *37* (19), 2659−2661.
(68) Lutz, F. T.; Gordon, B.; Kersten, M. G. Pericyclic Domino Reactions. In *Domino Reactions in Organic Synthesis*; John Wiley & Sons, Ltd: 2006; pp 280−336.
(69) Rickhaus, M.; Mayor, M.; Juríček, M. Chirality in Curved Polyaromatic Systems. *Chem. Soc. Rev.* **2017**, *46* (6), 1643−1660.
(70) Zha, G.-F.; Bare, G. A. L.; Leng, J.; Shang, Z.-P.; Luo, Z.; Qin, H.-L. Gram-Scale Synthesis of $\beta$-(Hetero)Arylethenesulfonyl Fluorides via a Pd(OAc)2 Catalyzed Oxidative Heck Process with DDQ or AgNO3 as an Oxidant. *Adv. Synth Catal* **2017**, *359* (18), 3237−3242.
(71) Lennox, A. J. J.; Lloyd-Jones, G. C. Selection of Boron Reagents for Suzuki−Miyaura Coupling. *Chem. Soc. Rev.* **2014**, *43* (1), 412−443.
(72) Perdew, J. P.; Burke, K.; Ernzerhof, M. Generalized Gradient Approximation Made Simple. *Phys. Rev. Lett.* **1996**, *77* (18), 3865−3868.
(73) Tkatchenko, A.; Scheffler, M. Accurate Molecular Van Der Waals Interactions from Ground-State Electron Density and Free-Atom Reference Data. *Phys. Rev. Lett.* **2009**, *102* (7), 73005.
(74) Ignatchenko, A. Launching Graphene into 3D-Space: Symmetry, Topology, and Strategies for Bottom-Up Synthesis of Schwarzites. *ChemRxiv*, **2024**,


https://doi.org/10.1021/acs.joc.4c01503
J. Org. Chem. 2025, 90, 971−983